Comparison of three-jet events in $p\bar{p}$ collisions at $\sqrt{s} = 1.8$ TeV to predictions from a next-to-leading order QCD calculation

D. Acosta,[14] T. Affolder,[7] M. G. Albrow,[13] D. Ambrose,[36] D. Amidei,[27] K. Anikeev,[26] J. Antos,[1] G. Apollinari,[13] T. Arisawa,[50] A. Artikov,[11] W. Ashmanskas,[2] F. Azfar,[34] P. Azzi-Bacchetta,[35] N. Bacchetta,[35] H. Bachacou,[24] W. Badgett,[13] A. Barbaro-Galtieri,[24] V. E. Barnes,[39] B. A. Barnett,[21] S. Baroiant,[5] M. Barone,[15] G. Bauer,[26] F. Bedeschi,[37] S. Behari,[21] S. Belforte,[47] W. H. Bell,[17] G. Bellettini,[37] J. Bellinger,[51] D. Benjamin,[12] A. Beretvas,[13] A. Bhatti,[41] M. Binkley,[13] D. Bisello,[35] M. Bishai,[13] R. E. Blair,[2] C. Blocker,[4] K. Bloom,[27] B. Blumenfeld,[21] A. Bocci,[41] A. Bodek,[40] G. Bolla,[39] A. Bolshov,[26] D. Bortoletto,[39] J. Boudreau,[38] C. Bromberg,[28] E. Brubaker,[24] J. Budagov,[11] H. S. Budd,[40] K. Burkett,[13] G. Busetto,[35] K. L. Byrum,[2] S. Cabrera,[12] M. Campbell,[27] W. Carithers,[24] D. Carlsmith,[51] A. Castro,[3] D. Cauz,[47] A. Cerri,[24] L. Cerrito,[20] J. Chapman,[27] C. Chen,[36] Y. C. Chen,[1] M. Chertok,[5] G. Chiarelli,[37] G. Chlachidze,[13] F. Chlebana,[13] M. L. Chu,[1] J. Y. Chung,[32] W.-H. Chung,[51] Y. S. Chung,[40] C. I. Ciobanu,[20] A. G. Clark,[16] M. Coca,[40] A. Connolly,[24] M. Convery,[41] J. Conway,[43] M. Cordelli,[15] J. Cranshaw,[45] R. Culbertson,[13] D. Dagenhart,[4] S. D'Auria,[17] P. de Barbaro,[40] S. De Cecco,[42] S. Dell'Agnello,[15] M. Dell'Orso,[37] S. Demers,[40] L. Demortier,[41] M. Deninno,[3] D. De Pedis,[42] P. F. Derwent,[13] C. Dionisi,[42] J. R. Dittmann,[13] A. Dominguez,[24] S. Donati,[37] M. D'Onofrio,[16] T. Dorigo,[35] N. Eddy,[20] R. Erbacher,[13] D. Errede,[20] S. Errede,[20] R. Eusebi,[40] S. Farrington,[17] R. G. Feild,[52] J. P. Fernandez,[39] C. Ferretti,[27] R. D. Field,[14] I. Fiori,[37] B. Flaugher,[13] L. R. Flores-Castillo,[38] G. W. Foster,[13] M. Franklin,[18] J. Friedman,[26] I. Furic,[26] M. Gallinaro,[41] A. F. Garfinkel,[39] C. Gay,[52] D. W. Gerdes,[27] E. Gerstein,[9] S. Giagu,[42] P. Giannetti,[37] K. Giolo,[39] M. Giordani,[47] P. Giromini,[15] V. Glagolev,[11] D. Glenzinski,[13] M. Gold,[30] N. Goldschmidt,[27] J. Goldstein,[34] G. Gomez,[8] M. Goncharov,[44] I. Gorelov,[30] A. T. Goshaw,[12] Y. Gotra,[38] K. Goulianos,[41] A. Gresele,[3] C. Grosso-Pilcher,[10] M. Guenther,[39] J. Guimaraes da Costa,[18] C. Haber,[24] S. R. Hahn,[13] E. Halkiadakis,[40] R. Handler,[51] F. Happacher,[15] K. Hara,[48] R. M. Harris,[13] F. Hartmann,[22] K. Hatakeyama,[41] J. Hauser,[6] J. Heinrich,[36] M. Hennecke,[22] M. Herndon,[21] C. Hill,[7] A. Hocker,[40] K. D. Hoffman,[10] S. Hou,[1] B. T. Huffman,[34] R. Hughes,[32] J. Huston,[28] J. Incandela,[7] G. Introzzi,[37] M. Iori,[42] C. Issever,[7] A. Ivanov,[40] Y. Iwata,[19] B. Iyutin,[26] E. James,[13] M. Jones,[39] T. Kamon,[44] J. Kang,[27] M. Karagoz Unel,[31] S. Kartal,[13] H. Kasha,[52] Y. Kato,[33] R. D. Kennedy,[13] R. Kephart,[13] B. Kilminster,[40] D. H. Kim,[23] H. S. Kim,[20] M. J. Kim,[9] S. B. Kim,[23] S. H. Kim,[48] T. H. Kim,[26] Y. K. Kim,[10] M. Kirby,[12] L. Kirsch,[4] S. Klimenko,[14] P. Koehn,[32] K. Kondo,[50] J. Konigsberg,[14] A. Korn,[26] A. Korytov,[14] J. Kroll,[36] M. Kruse,[12] V. Krutelyov,[44] S. E. Kuhlmann,[2] N. Kuznetsova,[13] A. T. Laasanen,[39] S. Lami,[41] S. Lammel,[13] J. Lancaster,[12] M. Lancaster,[25] R. Lander,[5] K. Lannon,[32] A. Lath,[43] G. Latino,[30] T. LeCompte,[2] Y. Le,[21] J. Lee,[40] S. W. Lee,[44] N. Leonardo,[26] S. Leone,[37] J. D. Lewis,[13] K. Li,[52] C. S. Lin,[13] M. Lindgren,[6] T. M. Liss,[20] D. O. Litvintsev,[13] T. Liu,[13] N. S. Lockyer,[36] A. Loginov,[29] M. Loreti,[35] D. Lucchesi,[35] P. Lukens,[13] L. Lyons,[34] J. Lys,[24] R. Madrak,[18] K. Maeshima,[13] P. Maksimovic,[21] L. Malferrari,[3] G. Manca,[34] M. Mangano,[37] M. Mariotti,[35] A. Martin,[52] M. Martin,[21] V. Martin,[31] M. Martínez,[13] P. Mazzanti,[3] K. S. McFarland,[40] P. McIntyre,[44] M. Menguzzato,[35] A. Menzione,[37] P. Merkel,[13] C. Mesropian,[41] A. Meyer,[13] T. Miao,[13] J. S. Miller,[27] R. Miller,[28] S. Miscetti,[15] G. Mitselmakher,[14] N. Moggi,[3] R. Moore,[13] T. Moulik,[39] A. Mukherjee,[13] M. Mulhearn,[26] T. Muller,[22] A. Munar,[36] P. Murat,[13] J. Nachtman,[13] S. Nahn,[52] I. Nakano,[19] R. Napora,[21] C. Nelson,[13] T. Nelson,[13] C. Neu,[32] M. S. Neubauer,[26] C. Newman-Holmes,[13] F. Niell,[27] T. Nigmanov,[38] L. Nodulman,[2] S. H. Oh,[12] Y. D. Oh,[23] T. Ohsugi,[19] T. Okusawa,[33] W. Orejudos,[24] C. Pagliarone,[37] F. Palmonari,[37] R. Paoletti,[37] V. Papadimitriou,[45] J. Patrick,[13] G. Pauletta,[47] M. Paulini,[9] T. Pauly,[34] C. Paus,[26] D. Pellett,[5] A. Penzo,[47] T. J. Phillips,[12] G. Piacentino,[37] J. Piedra,[8] K. T. Pitts,[20] A. Pompoš,[39] L. Pondrom,[51] G. Pope,[38] O. Poukhov,[11] T. Pratt,[34] F. Prokoshin,[11] J. Proudfoot,[2] F. Ptohos,[15] G. Punzi,[37] J. Rademacker,[34] A. Rakitine,[26] F. Ratnikov,[43] H. Ray,[27] A. Reichold,[34] P. Renton,[34] M. Rescigno,[42] F. Rimondi,[3] L. Ristori,[37] W. J. Robertson,[12] T. Rodrigo,[8] S. Rolli,[49] L. Rosenson,[26] R. Roser,[13] R. Rossin,[35] C. Rott,[39] A. Roy,[39] A. Ruiz,[8] D. Ryan,[49] A. Safonov,[5] R. St. Denis,[17] W. K. Sakumoto,[40] D. Saltzberg,[6] C. Sanchez,[32] A. Sansoni,[15] L. Santi,[47] S. Sarkar,[42] P. Savard,[46] A. Savoy-Navarro,[13] P. Schlabach,[13] E. E. Schmidt,[13] M. P. Schmidt,[52] M. Schmitt,[31] L. Scodellaro,[35] A. Scribano,[37] A. Sedov,[39] S. Seidel,[30] Y. Seiya,[48] A. Semenov,[11] F. Semeria,[3] M. D. Shapiro,[24] P. F. Shepard,[38] T. Shibayama,[48] M. Shimojima,[48] M. Shochet,[10] A. Sidoti,[35] A. Sill,[45] P. Sinervo,[46] A. J. Slaughter,[52] K. Sliwa,[49] F. D. Snider,[13] R. Snihur,[25] M. Spezziga,[45] L. Spiegel,[13] F. Spinella,[37] M. Spiropulu,[7] A. Stefanini,[37] J. Strologas,[30] D. Stuart,[7] A. Sukhanov,[14] K. Sumorok,[26] T. Suzuki,[48] R. Takashima,[19] K. Takikawa,[48] M. Tanaka,[2] M. Tecchio,[27] P. K. Teng,[1] K. Terashi,[41] R. J. Tesarek,[13] S. Tether,[26] J. Thom,[13] T. L. Thomas,[30,*] A. S. Thompson,[17] E. Thomson,[32] P. Tipton,[40] S. Tkaczyk,[13] D. Toback,[44] K. Tollefson,[28] D. Tonelli,[37] M. Tönnesmann,[28] H. Toyoda,[33] W. Trischuk,[46] J. Tseng,[26] D. Tsybychev,[14] N. Turini,[37] F. Ukegawa,[48] T. Unverhau,[17] T. Vaiciulis,[40] A. Varganov,[27] E. Vataga,[37] S. Vejcik III,[13] G. Velev,[13] G. Veramendi,[24] R. Vidal,[13] I. Vila,[8] R. Vilar,[8]

I. Volobouev,[24] M. von der Mey,[6] R. G. Wagner,[2] R. L. Wagner,[13] W. Wagner,[22] Z. Wan,[43] C. Wang,[12] M. J. Wang,[1] S. M. Wang,[14] B. Ward,[17] S. Waschke,[17] D. Waters,[25] T. Watts,[43] M. Weber,[24] W. C. Wester III,[13] B. Whitehouse,[49] A. B. Wicklund,[2] E. Wicklund,[13] H. H. Williams,[36] P. Wilson,[13] B. L. Winer,[32] S. Wolbers,[13] M. Wolter,[49] S. Worm,[43] X. Wu,[16] F. Würthwein,[26] U. K. Yang,[10] W. Yao,[24] G. P. Yeh,[13] K. Yi,[21] J. Yoh,[13] T. Yoshida,[33] I. Yu,[23] S. Yu,[36] J. C. Yun,[13] L. Zanello,[42] A. Zanetti,[47] F. Zetti,[24] and S. Zucchelli[3]

[1]*Institute of Physics, Academia Sinica, Taipei, Taiwan 11529, Republic of China*
[2]*Argonne National Laboratory, Argonne, Illinois 60439, U.S.A.*
[3]*Istituto Nazionale di Fisica Nucleare, University of Bologna, I-40127 Bologna, Italy*
[4]*Brandeis University, Waltham, Massachusetts 02254, U.S.A.*
[5]*University of California at Davis, Davis, California 95616, U.S.A.*
[6]*University of California at Los Angeles, Los Angeles, California 90024, U.S.A.*
[7]*University of California at Santa Barbara, Santa Barbara, California 93106, U.S.A.*
[8]*Instituto de Fisica de Cantabria, CSIC-University of Cantabria, 39005 Santander, Spain*
[9]*Carnegie Mellon University, Pittsburgh, Pennsylvania 15213, U.S.A.*
[10]*Enrico Fermi Institute, University of Chicago, Chicago, Illinois 60637, U.S.A.*
[11]*Joint Institute for Nuclear Research, RU-141980 Dubna, Russia*
[12]*Duke University, Durham, North Carolina 27708, U.S.A.*
[13]*Fermi National Accelerator Laboratory, Batavia, Illinois 60510, U.S.A.*
[14]*University of Florida, Gainesville, Florida 32611, U.S.A.*
[15]*Laboratori Nazionali di Frascati, Istituto Nazionale di Fisica Nucleare, I-00044 Frascati, Italy*
[16]*University of Geneva, CH-1211 Geneva 4, Switzerland*
[17]*Glasgow University, Glasgow G12 8QQ, United Kingdom*
[18]*Harvard University, Cambridge, Massachusetts 02138, U.S.A.*
[19]*Hiroshima University, Higashi-Hiroshima 724, Japan*
[20]*University of Illinois, Urbana, Illinois 61801, U.S.A.*
[21]*The Johns Hopkins University, Baltimore, Maryland 21218, U.S.A.*
[22]*Institut für Experimentelle Kernphysik, Universität Karlsruhe, 76128 Karlsruhe, Germany*
[23]*Center for High Energy Physics: Kyungpook National University, Taegu 702-701; Seoul National University, Seoul 151-742; and SungKyunKwan University, Suwon 440-746; Korea*
[24]*Ernest Orlando Lawrence Berkeley National Laboratory, Berkeley, California 94720, U.S.A.*
[25]*University College London, London WC1E 6BT, United Kingdom*
[26]*Massachusetts Institute of Technology, Cambridge, Massachusetts 02139, U.S.A.*
[27]*University of Michigan, Ann Arbor, Michigan 48109, U.S.A.*
[28]*Michigan State University, East Lansing, Michigan 48824, U.S.A.*
[29]*Institution for Theoretical and Experimental Physics, ITEP, Moscow 117259, Russia*
[30]*University of New Mexico, Albuquerque, New Mexico 87131, U.S.A.*
[31]*Northwestern University, Evanston, Illinois 60208, U.S.A.*
[32]*The Ohio State University, Columbus, Ohio 43210, U.S.A.*
[33]*Osaka City University, Osaka 588, Japan*
[34]*University of Oxford, Oxford OX1 3RH, United Kingdom*
[35]*Universita di Padova, Istituto Nazionale di Fisica Nucleare, Sezione di Padova, I-35131 Padova, Italy*
[36]*University of Pennsylvania, Philadelphia, Pennsylvania 19104, U.S.A.*
[37]*Istituto Nazionale di Fisica Nucleare, University and Scuola Normale Superiore of Pisa, I-56100 Pisa, Italy*
[38]*University of Pittsburgh, Pittsburgh, Pennsylvania 15260, U.S.A.*
[39]*Purdue University, West Lafayette, Indiana 47907*
[40]*University of Rochester, Rochester, New York 14627, U.S.A.*
[41]*Rockefeller University, New York, New York 10021, U.S.A.*
[42]*Instituto Nazionale de Fisica Nucleare, Sezione di Roma, University di Roma I, "La Sapienza," I-00185 Roma, Italy*
[43]*Rutgers University, Piscataway, New Jersey 08855, U.S.A.*
[44]*Texas A&M University, College Station, Texas 77843, U.S.A.*
[45]*Texas Tech University, Lubbock, Texas 79409, U.S.A.*
[46]*Institute of Particle Physics, University of Toronto, Toronto M5S 1A7, Canada*
[47]*Istituto Nazionale di Fisica Nucleare, University of Trieste/Udine, Italy*
[48]*University of Tsukuba, Tsukuba, Ibaraki 305, Japan*
[49]*Tufts University, Medford, Massachusetts 02155, U.S.A.*
[50]*Waseda University, Tokyo 169, Japan*
[51]*University of Wisconsin, Madison, Wisconsin 53706, U.S.A.*

*Visitor

[52]*Yale University, New Haven, Connecticut 06520, U.S.A.*
(Received 15 September 2004; published 4 February 2005)

The properties of three-jet events with total transverse energy greater than 320 GeV and individual jet energy greater than 20 GeV have been analyzed and compared to absolute predictions from a next-to-leading order (NLO) perturbative QCD calculation. These data, of integrated luminosity 86 pb^{-1}, were recorded by the CDF Experiment for $p\overline{p}$ collisions at $\sqrt{s} = 1.8$ TeV. This study tests a model of higher order QCD processes that result in gluon emission and may give some indication of the magnitude of the contribution of processes higher than NLO. The total cross section is measured to be $466 \pm 3(\mathrm{stat.})^{+207}_{-70}(\mathrm{syst.})$ pb. The differential cross section is furthermore measured for all kinematically accessible regions of the Dalitz plane, including those for which the theoretical prediction is unreliable. While the measured cross section is consistent with the theoretical prediction in magnitude, the two differ somewhat in shape in the Dalitz plane.

DOI: 10.1103/PhysRevD.71.032002 PACS numbers: 12.38.Qk

In perturbative QCD, hard scattering of the constituent partons in the proton and antiproton results in events with large total transverse energy, $\sum E_{\mathrm{T}}$. Outgoing scattered partons hadronize and may be detected as hadronic jets. Three-jet events can be produced when a hard gluon is radiated from any of the initial, intermediate, or final state partons in an event with two primary outgoing partons.

We analyze here some properties of the cross section for three-jet event production in proton-antiproton collisions at the Fermilab Tevatron Collider at center-of-mass energy 1.8 TeV. The data, which were recorded by the Collider Detector at Fermilab (CDF) [1], are compared with predictions of the first complete next-to-leading order (NLO) QCD generator, Trirad [2], for hadronic three-jet production at hadron colliders. We compare the measured and predicted absolute cross sections to test our understanding of the higher order QCD processes that result in gluon emission and to estimate the magnitude of the contribution of processes higher than NLO.[2] In some kinematical regions, we provide a measurement of the cross section where the theoretical prediction is not reliable; this measurement may be a useful guide for theoretical calculations. We also compared the shapes of the measured and predicted cross sections when normalized, to examine the sensitivity of the cross section to variations in the value of the strong coupling, α_{s}. The data sample corresponds to an integrated luminosity of 86 pb^{-1} collected during the 1994-1995 run (Run 1b).

A previous paper [4] examined a smaller dataset and was limited to a comparison with leading order theoretical calculations [5]. A subsequent analysis [6] compared a larger dataset to predictions from the HERWIG [7] parton shower Monte Carlo program and to the NJETS [8] leading order $2 \rightarrow N$ parton-level prediction. The NLO calculation used here has the benefit of reduced renormalization scale dependence (and consequently lower systematic uncertainty) as well as a more reliable description of multijet production throughout phase space. This study expands upon the previous investigations by comparing the data to absolute cross section predictions. The measurements presented here include differential cross sections that may provide useful constraints upon parton distribution functions.

We use a coordinate system with the z axis along the proton beam, transverse coordinate perpendicular to the beam, azimuthal angle ϕ, polar angle θ, and pseudorapidity $\eta = -\ln \tan(\theta/2)$. The analysis uses the CDF calorimeters [9], which cover the pseudorapidity range $|\eta| < 4.2$. The calorimeters are constructed in a tower geometry and are segmented in depth into electromagnetic and hadronic components. The calorimeter towers are 0.1 units wide in η. The tower widths in ϕ are 15° in the central region and 5° for $|\eta|$ greater than approximately 1.2.

We begin by considering events from the data sample selected by the trigger requirement $\sum E_{\mathrm{T}} > 175$ GeV. We refer to this 175 GeV as $E_{\mathrm{tot}}^{\mathrm{thr}}$ below. Event reconstruction uses a cone algorithm [4] described in more detail below. The transverse energy is defined as $E_{\mathrm{T}} \equiv E\sin\theta$, where E is the scalar sum of energy deposited in the calorimeter within a particular cone and θ is the angle between the beam direction in the laboratory frame and the cone axis. All calorimeter energy clusters [4] in the event with $E_{\mathrm{T}} > 10$ GeV are summed. The three leading jets in the laboratory frame are used as the basis of transformation into the three-jet rest frame. In the three-jet rest frame, the incoming partons are, by convention [10], labeled partons 1 and 2, and their momenta are designated $\vec{p}_1$ and $\vec{p}_2$, respectively. The highest energy jets in this frame have energies labeled E_3, E_4, and E_5 and are ordered such that $E_3 > E_4 > E_5$. The outgoing partons associated with these jets are correspondingly labeled partons 3, 4, and 5.

A three-jet system in the massless parton approximation can be uniquely described by five independent variables (see Figure 5 in [11]). We use the following:

(1) the invariant mass of the three-jet system, $m_{3\mathrm{J}}$

[2]While no quantitative estimate of the contribution of next-to-next-to-leading order processes to the cross section is available at this time, considerable progress has recently been made in calculating two loop $2 \rightarrow 2$ parton processes [3], important groundwork for the future.

(2) the cosine of the angle θ_3^* between the average beam direction ($\vec{p}_{\rm AV} \equiv \vec{p}_1 - \vec{p}_2$) and parton 3 in the three-jet rest frame:

$$\cos\theta_3^* \equiv \frac{\vec{p}_{\rm AV} \cdot \vec{p}_3}{|\vec{p}_{\rm AV}||\vec{p}_3|}$$

(3) the cosine of the angle ψ^* between the plane containing the average beam direction and parton 3 and the plane containing partons 3, 4, and 5 in their center of mass frame:

$$\cos\psi^* \equiv \frac{(\vec{p}_3 \times \vec{p}_{\rm AV}) \cdot (\vec{p}_4 \times \vec{p}_5)}{|\vec{p}_3 \times \vec{p}_{\rm AV}||\vec{p}_4 \times \vec{p}_5|}$$

(4) the Dalitz variable X_3 (see below) for the leading jet, and

(5) the Dalitz variable X_4 (see below) for the next-to-leading jet.

The invariant $m_{3\rm J}$ is calculated by sorting jets by their energies in the laboratory frame, boosting to the rest frame of those with the three highest energies, re-sorting jets by energy in that frame, then computing $m_{3\rm J} = \sum_{i=3}^{5} E_{\rm i}$, where the $E_{\rm i}$ are the energies of jets 3, 4, and 5 in the rest frame. We have investigated the probability that a jet with energy less than the weakest of the three jets in the laboratory frame may have an energy greater than E_5 in the 3-jet rest frame from which it is excluded by this algorithm. The restriction imposed by the cut on full trigger efficiency (see below) makes this probability negligible.

The Dalitz variables, $X_{\rm i}$, are defined as $X_{\rm i} \equiv 2 \cdot E_{\rm i}/m_{3\rm J}$, $(i = 3, 4, 5)$. Momentum conservation restricts the ranges of the Dalitz variables to

$$\frac{2}{3} \le X_3 \le 1, \qquad \frac{1}{2} \le X_4 \le 1, \text{ and} \qquad 0 \le X_5 \le \frac{2}{3}.$$

A set of trigger and offline requirements [12] rejects events associated with cosmic rays, beam halo, and calorimeter malfunctions. Events are required to have a reconstructed primary vertex, defined as the vertex with the largest $\sum_i P_{\rm i}$ (where $P_{\rm i}$ is the total momentum of particle i leaving the vertex in the event), within $|z| < 60$ cm. Events are defined to have resolved multiple interactions if a second vertex with at least ten associated tracks is reconstructed in the vertex track detector, and if that vertex is separated from the primary one by at least 10 cm. Because multiple interactions can change the jet multiplicity in an event, for example, misidentifying two-jet events as three-jet events, events with resolved multiple interactions are removed. No correction is applied for the number of events with unresolved multiple interactions, which was estimated by the following method to constitute less than 2% of the data set. The multiplicity distribution of events with resolved multiple interactions was subtracted from that of the complete inclusive three-jet dataset, yielding the multiplicity distribution for the combined dataset of single interactions and unresolved multiple interactions. The mean jet multiplicity for this "Single + Unresolved Multiple" dataset was graphed as a function of instantaneous luminosity. The mean multiplicity of this dataset, excluding that due to events with unresolved multiple interactions, was determined by extrapolating the distribution to zero luminosity. The difference between that extrapolated multiplicity and the multiplicity of the full Single + Unresolved Multiple dataset was then converted to an event number excess (less than 2%) with a Poissonian Monte Carlo program. The effective total integrated luminosity of the full data sample is 77 ± 4 pb^{-1}, where the uncertainty reflects both the overall luminosity uncertainty (4.2%) and the uncertainty (0.5%) associated with the removal of resolved multiple interactions.

The data, which involve jet properties, can be compared to NLO parton level predictions through the use of a clustering algorithm which can be implemented for both [13] in combination with jet energy corrections. Both of those procedures are reviewed in [14]; their essential elements are summarized here.

An iterative cone algorithm [4] with cone radius $R \equiv \sqrt{(\Delta\eta)^2 + (\Delta\phi)^2} = 0.7$ is used to identify jets. Here $\Delta\eta = \eta_2 - \eta_1$ and $\Delta\phi = \phi_2 - \phi_1$. The subscripts 1 and 2 correspond to the axes of the cone and calorimeter tower, respectively. Jets that share towers are combined if the total $E_{\rm T}$ of the shared towers is greater than 75% of the $E_{\rm T}$ of either jet; otherwise the towers are assigned to the nearest jet. Jet energies are corrected [4] for errors in the absolute and relative energy scales and for additional energy associated with the underlying event. Since partons that are radiated out of the cone lead to the same losses in the theoretical calculation and in the data, out-of-cone corrections are not applied. The $E_{\rm T}$ of a jet is calculated from the reconstructed position of the primary event vertex. All three leading jets are required to have $E_{\rm T} > 20$ GeV and $|\eta| < 2.0$. Events with fewer than three jets are rejected. To avoid collinear soft gluon instability in the iterative jet clustering algorithm [15], a cone overlap cut is imposed: events are rejected if the distance ΔR in η-ϕ space between the axes of any two of the three leading jets is less than 1.0 (see Figure 5 of [4], which shows that this selection requirement reduces to approximately zero the probability of the two jets being merged by the clustering algorithm). To exclude regions in which the geometrical acceptance [11] is less than about 95%, we require $|\cos\theta_3^*| < \sqrt{1 - (E_{\rm tot}^{\rm thr}/{\rm c}^2/m_{2\rm J})^2}$, where $m_{2\rm J}$ is the mass of the two leading jets in the three-jet system and is defined analogously to $m_{3\rm J}$.

We require full trigger efficiency, which occurs when $\sum_{\rm 3jets} E_{\rm T} > 320$ GeV, where the sum is over the three highest energy jets in the event with corrected $E_{\rm T} > 20$ GeV [16]. The data are compared to the theoretical prediction by

sorting events into bins of size 0.02×0.02 in X_3-X_4 space, the Dalitz plane. Figure 1 shows the Dalitz distribution of data that remain after all of the selection requirements have been applied.

Before the final binning is done, the data are corrected for the effects of the combination of detector resolution and energy mismeasurement. A correction factor is determined for each bin in the plane as follows. A sample of events is generated at the parton level with the HERWIG Monte Carlo. The final state partons are hadronized. The events are then binned in the Dalitz plane. The same events are next passed through the CDF detector simulation and rebinned. For each bin the ratio of the number of events after and before detector simulation is computed. This ratio (ranging from 0.85 to 1.5, with 74% of the values lying in the range 0.9 to 1.1) is the factor subsequently used to correct the number of events in each data bin. The high quality of correspondence between the HERWIG events and the data was validated in two ways. An independent set of HERWIG events was generated, simulated, and then corrected using the correction factors obtained above. The agreement between the resulting corrected simulated events and their true (pre-simulation) X_3 and X_4 values was found to be excellent. In addition we reverified for this paper's dataset the agreement between data and HERWIG for distributions of m_{3J}, X_3, and X_4 that was previously demonstrated in Figures 1, 3a, and 3b, respectively, of Ref. [6]. The data are also corrected for the z-vertex cut

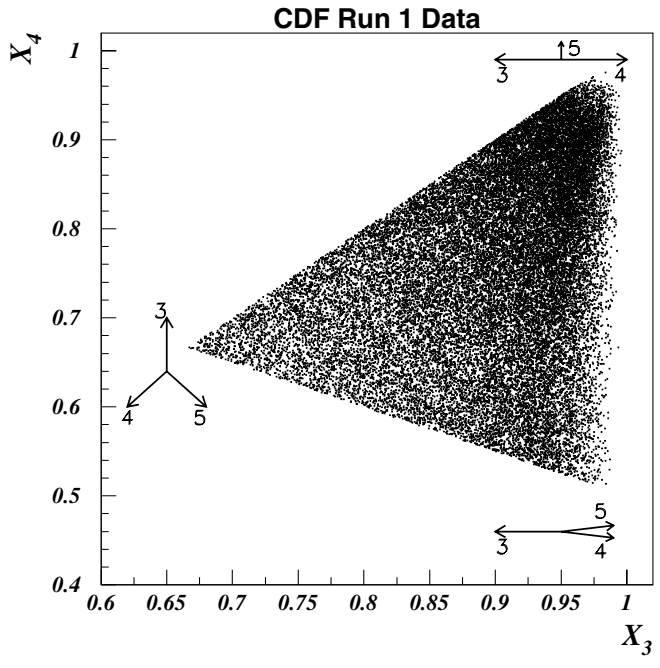

FIG. 1. The three-jet data, after all selection requirements have been applied. The energy correction procedure (see text) has not been applied. The figures at the corners of the distribution represent typical three-jet topologies in those regions of the Dalitz plane.

efficiency and then normalized to the effective total luminosity.

The principal sources of systematic uncertainty [17] on the cross section are those on the absolute and relative (η-dependent) jet energy scales. The uncertainty on absolute jet energy derives from the resolution on the calibration of the calorimeter (uncertainty 1.3%–1.8%, and E_T-dependent), the uncertainty associated with choice of jet fragmentation model (decreasing from 1.7% to 1.2% with increasing E_T), the uncertainty associated with calorimeter stability over time (1%), and the uncertainty on the correction for the contribution of the underlying event (1 GeV). The uncertainty on the relative jet energy scale ranges from 2% to 6%. Uncertainties are also associated with the measurement of the effective total integrated luminosity (4.2%) and with the z-vertex cut efficiency (2%). There is also an uncertainty of less than 5% associated with the implementation of simulated events in the correction procedure.

The uncertainty due to the jet fragmentation model was determined by comparing the transverse momentum spectra of charged particles in measured jets using tracking information to the same information for events generated with ISAJET [18], which has Feynman-Field fragmentation implemented. The spectra were checked with HERWIG events and found to be consistent. The uncertainty stems from the uncertainty on track reconstruction [14]. The uncertainty due to choice of Monte Carlo generator was studied by comparing the jet characteristics of data with those of HERWIG and PYTHIA [19] events. The difference between the spectra was found to be smaller than the uncertainty due to the jet fragmentation model, and the associated uncertainty is neglected here.

The upper (lower) limits on all these uncertainties are added (subtracted) from the four-momenta of the jets in the data sample to obtain the systematic uncertainties on the cross section associated with each contribution. The uncertainties are then combined to produce the total experimental systematic uncertainty reported for each bin in Tables I, II, III, IV, V, VI, VII, VIII, IX, X, XI, XII, XIII, and XIV below.

The Trirad calculation consists of $2 \rightarrow 3$ parton processes at one loop and $2 \rightarrow 4$ parton processes at tree level. For gluons g, incoming quarks q, and outgoing quarks Q or Q', the subprocesses involved are $gg \rightarrow ggg$, $\overline{q}q \rightarrow ggg$, $\overline{q}q \rightarrow \overline{Q}Qg$, and those related by crossing symmetry, all computed to one loop; and $gg \rightarrow gggg$, $\overline{q}q \rightarrow gggg$, $\overline{q}q \rightarrow \overline{Q}Qgg$, and $\overline{q}q \rightarrow \overline{Q}Q\overline{Q}'Q'$ and the crossed processes computed at tree level. The program uses the ''subtraction improved'' [15] phase space slicing method to implement infrared cancellation.

The cross section is predicted with the CTEQ4M [20] parton distribution function (PDF) for each bin in the Dalitz plane. The result is multiplied by the effective total integrated luminosity of the data to predict a number of

TABLE I. The measured and predicted three-jet production cross section in every kinematically allowed bin in the Dalitz plane as a function of X_3 and X_4.

X_3	X_4	Measured Cross Section (pb)	NLO Cross Section CTEQ4M (pb)
0.67	0.67	$0.5^{+0.3}_{-0.2}$	0.4 ± 0.1
0.69	0.65	$0.3^{+0.1}_{-0.2}$	0.2 ± 0.1
0.69	0.67	$1.4^{+0.9}_{-0.4}$	1.4 ± 0.1
0.69	0.69	$0.7^{+0.4}_{-0.1}$	0.6 ± 0.1
0.71	0.65	$1.0^{+0.5}_{-0.2}$	1.0 ± 0.1
0.71	0.67	$1.3^{+0.6}_{-0.2}$	1.2 ± 0.1
0.71	0.69	$1.6^{+0.6}_{-0.2}$	1.2 ± 0.1
0.71	0.71	$0.9^{+0.4}_{-0.2}$	0.7 ± 0.1
0.73	0.63	$0.2^{+0.1}_{-0.1}$	0.3 ± 0.1
0.73	0.65	$1.3^{+0.6}_{-0.2}$	1.3 ± 0.1
0.73	0.67	$1.4^{+0.6}_{-0.2}$	1.2 ± 0.1
0.73	0.69	$1.4^{+0.8}_{-0.2}$	1.4 ± 0.1
0.73	0.71	$1.5^{+0.8}_{-0.3}$	1.6 ± 0.1
0.73	0.73	$0.7^{+0.3}_{-0.2}$	0.5 ± 0.1
0.75	0.63	$0.9^{+0.5}_{-0.2}$	0.9 ± 0.1
0.75	0.65	$1.3^{+0.7}_{-0.2}$	1.3 ± 0.1

TABLE II. The measured and predicted three-jet production cross section in every kinematically allowed bin in the Dalitz plane as a function of X_3 and X_4.

X_3	X_4	Measured Cross Section (pb)	NLO Cross Section CTEQ4M (pb)
0.75	0.67	$1.2^{+0.7}_{-0.3}$	1.4 ± 0.1
0.75	0.69	$1.7^{+0.8}_{-0.2}$	1.3 ± 0.1
0.75	0.71	$2.1^{+0.8}_{-0.4}$	1.4 ± 0.1
0.75	0.73	$2.0^{+0.8}_{-0.3}$	1.6 ± 0.1
0.75	0.75	$0.8^{+0.5}_{-0.1}$	0.9 ± 0.1
0.77	0.61	$0.4^{+0.3}_{-0.2}$	0.3 ± 0.1
0.77	0.63	$1.5^{+0.6}_{-0.2}$	1.4 ± 0.1
0.77	0.65	$1.7^{+0.8}_{-0.3}$	1.5 ± 0.1
0.77	0.67	$1.5^{+0.6}_{-0.2}$	1.4 ± 0.1
0.77	0.69	$1.7^{+0.8}_{-0.4}$	1.3 ± 0.1
0.77	0.71	$1.5^{+0.7}_{-0.2}$	1.4 ± 0.1
0.77	0.73	$1.5^{+0.8}_{-0.3}$	1.6 ± 0.1
0.77	0.75	$2.0^{+0.9}_{-0.3}$	1.6 ± 0.1
0.77	0.77	$1.1^{+0.5}_{-0.2}$	0.9 ± 0.1
0.79	0.61	$1.0^{+0.6}_{-0.2}$	1.0 ± 0.1
0.79	0.63	$1.6^{+0.8}_{-0.2}$	1.5 ± 0.1

events in each bin. We restrict the prediction to bins for which $X_3 < 0.98$; this is necessary as the perturbative expansion is not reliable where the three-jet configuration approaches a two-jet configuration. The comparison between the data and the calculation is made for 215 bins.

Figure 2 compares Dalitz distributions of the data and the absolute theoretical prediction. The theoretical distribution is more strongly peaked—a trend that persists in comparisons with all members of the CTEQ4 family[3] of PDFs. This trend, in which the edges of the Dalitz plane are more populated by data than by the prediction, may give some indication of the size of the higher order contributions to the cross section.

The data and theory are compared in two different ways. In Fig. 3, we compare the shapes of their Dalitz distributions by normalizing the data and theory predictions to the same number of events. In Fig. 4, we normalize theory to the experimental luminosity and compare the absolute values of the cross sections that are observed and predicted. In both figures, the prediction is made using the CTEQ4M parton distribution function, and the difference between observed and predicted number of events, scaled by the number of predicted events, is computed.

[3]The CTEQ4 family includes CTEQ4A1, CTEQ4A2, CTEQ4M, CTEQ4A4, and CTEQ4A5, which differ in the value of α_s input to their global fit, and CTEQ4HJ, for which a higher statistical emphasis was given to the high E_T data from CDF.

TABLE III. The measured and predicted three-jet production cross section in every kinematically allowed bin in the Dalitz plane as a function of X_3 and X_4.

X_3	X_4	Measured Cross Section (pb)	NLO Cross Section CTEQ4M (pb)
0.79	0.65	$1.7^{+0.8}_{-0.4}$	1.3 ± 0.1
0.79	0.67	$1.5^{+0.8}_{-0.3}$	1.6 ± 0.1
0.79	0.69	$1.8^{+0.7}_{-0.2}$	1.4 ± 0.1
0.79	0.71	$1.8^{+0.8}_{-0.3}$	1.5 ± 0.1
0.79	0.73	$1.7^{+0.6}_{-0.3}$	1.7 ± 0.2
0.79	0.75	$1.8^{+0.9}_{-0.5}$	1.8 ± 0.2
0.79	0.77	$1.8^{+1.2}_{-0.5}$	1.7 ± 0.1
0.79	0.79	$1.0^{+0.3}_{-0.2}$	1.0 ± 0.1
0.81	0.59	$0.4^{+0.3}_{-0.1}$	0.3 ± 0.1
0.81	0.61	$1.4^{+0.7}_{-0.3}$	1.6 ± 0.1
0.81	0.63	$1.6^{+0.6}_{-0.2}$	1.6 ± 0.1
0.81	0.65	$1.8^{+0.8}_{-0.3}$	1.5 ± 0.1
0.81	0.67	$2.0^{+0.7}_{-0.3}$	1.9 ± 0.2
0.81	0.69	$1.5^{+0.8}_{-0.2}$	1.7 ± 0.1
0.81	0.71	$1.7^{+0.9}_{-0.4}$	1.5 ± 0.1
0.81	0.73	$1.8^{+0.6}_{-0.2}$	1.9 ± 0.2

TABLE IV. The measured and predicted three-jet production cross section in every kinematically allowed bin in the Dalitz plane as a function of X_3 and X_4.

X_3	X_4	Measured Cross Section (pb)	NLO Cross Section CTEQ4M (pb)
0.81	0.75	$2.2^{+0.8}_{-0.4}$	1.6 ± 0.1
0.81	0.77	$2.1^{+1.0}_{-0.3}$	2.2 ± 0.2
0.81	0.79	$2.5^{+1.3}_{-0.5}$	2.1 ± 0.2
0.81	0.81	$1.1^{+0.6}_{-0.2}$	1.1 ± 0.1
0.83	0.59	$1.3^{+0.9}_{-0.2}$	1.1 ± 0.1
0.83	0.61	$1.6^{+1.0}_{-0.4}$	1.7 ± 0.1
0.83	0.63	$1.8^{+0.6}_{-0.3}$	1.7 ± 0.2
0.83	0.65	$1.5^{+0.5}_{-0.2}$	1.6 ± 0.1
0.83	0.67	$1.6^{+1.0}_{-0.3}$	1.7 ± 0.2
0.83	0.69	$1.8^{+0.9}_{-0.4}$	1.9 ± 0.2
0.83	0.71	$2.1^{+1.1}_{-0.4}$	1.7 ± 0.2
0.83	0.73	$2.1^{+1.0}_{-0.3}$	2.0 ± 0.2
0.83	0.75	$2.2^{+0.9}_{-0.3}$	2.0 ± 0.2
0.83	0.77	$2.3^{+1.1}_{-0.2}$	2.0 ± 0.2
0.83	0.79	$2.2^{+0.8}_{-0.4}$	2.3 ± 0.2
0.83	0.81	$2.6^{+1.2}_{-0.3}$	2.4 ± 0.2

TABLE V. The measured and predicted three-jet production cross section in every kinematically allowed bin in the Dalitz plane as a function of X_3 and X_4.

X_3	X_4	Measured Cross Section (pb)	NLO Cross Section CTEQ4M (pb)
0.83	0.83	$1.3^{+0.6}_{-0.2}$	1.3 ± 0.1
0.85	0.57	$0.3^{+0.2}_{-0.1}$	0.3 ± 0.1
0.85	0.59	$2.2^{+1.1}_{-0.3}$	2.1 ± 0.2
0.85	0.61	$1.5^{+1.0}_{-0.5}$	1.5 ± 0.1
0.85	0.63	$1.8^{+0.8}_{-0.4}$	1.9 ± 0.2
0.85	0.65	$1.8^{+0.8}_{-0.3}$	1.7 ± 0.1
0.85	0.67	$2.2^{+1.0}_{-0.3}$	1.8 ± 0.2
0.85	0.69	$2.0^{+0.9}_{-0.3}$	1.7 ± 0.2
0.85	0.71	$2.4^{+0.9}_{-0.3}$	1.9 ± 0.2
0.85	0.73	$2.3^{+1.0}_{-0.4}$	2.1 ± 0.2
0.85	0.75	$2.1^{+1.3}_{-0.5}$	2.3 ± 0.2
0.85	0.77	$2.2^{+1.1}_{-0.5}$	2.3 ± 0.2
0.85	0.79	$2.3^{+1.1}_{-0.3}$	2.4 ± 0.2
0.85	0.81	$2.5^{+1.0}_{-0.4}$	2.8 ± 0.2
0.85	0.83	$3.0^{+1.4}_{-0.5}$	3.0 ± 0.2
0.85	0.85	$1.1^{+0.8}_{-0.2}$	1.5 ± 0.1

TABLE VI. The measured and predicted three-jet production cross section in every kinematically allowed bin in the Dalitz plane as a function of X_3 and X_4.

X_3	X_4	Measured Cross Section (pb)	NLO Cross Section CTEQ4M (pb)
0.87	0.57	$1.3^{+0.8}_{-0.2}$	1.4 ± 0.1
0.87	0.59	$2.0^{+1.1}_{-0.4}$	1.8 ± 0.2
0.87	0.61	$1.8^{+1.1}_{-0.5}$	1.7 ± 0.2
0.87	0.63	$2.0^{+1.4}_{-0.6}$	1.8 ± 0.2
0.87	0.65	$1.8^{+0.9}_{-0.3}$	1.9 ± 0.2
0.87	0.67	$1.9^{+1.3}_{-0.6}$	2.0 ± 0.2
0.87	0.69	$2.2^{+1.0}_{-0.4}$	2.2 ± 0.2
0.87	0.71	$2.2^{+1.3}_{-0.5}$	2.1 ± 0.2
0.87	0.73	$2.6^{+0.9}_{-0.4}$	2.2 ± 0.2
0.87	0.75	$2.6^{+1.3}_{-0.4}$	2.6 ± 0.2
0.87	0.77	$2.6^{+1.4}_{-0.6}$	2.5 ± 0.2
0.87	0.79	$2.5^{+1.3}_{-0.4}$	2.6 ± 0.2
0.87	0.81	$2.9^{+1.3}_{-0.3}$	3.5 ± 0.2
0.87	0.83	$3.0^{+1.5}_{-0.6}$	3.5 ± 0.2
0.87	0.85	$3.2^{+1.4}_{-0.4}$	3.1 ± 0.2
0.87	0.87	$1.5^{+0.6}_{-0.2}$	1.9 ± 0.2

TABLE VII. The measured and predicted three-jet production cross section in every kinematically allowed bin in the Dalitz plane as a function of X_3 and X_4.

X_3	X_4	Measured Cross Section (pb)	NLO Cross Section CTEQ4M (pb)
0.89	0.55	$0.6^{+0.2}_{-0.2}$	0.4 ± 0.1
0.89	0.57	$2.2^{+0.9}_{-0.3}$	1.9 ± 0.2
0.89	0.59	$1.8^{+1.1}_{-0.5}$	2.1 ± 0.2
0.89	0.61	$2.3^{+1.3}_{-0.5}$	1.8 ± 0.2
0.89	0.63	$2.5^{+1.3}_{-0.4}$	2.1 ± 0.2
0.89	0.65	$2.2^{+1.1}_{-0.6}$	2.3 ± 0.2
0.89	0.67	$2.2^{+1.4}_{-0.4}$	2.3 ± 0.2
0.89	0.69	$2.6^{+1.6}_{-0.5}$	2.4 ± 0.2
0.89	0.71	$2.8^{+1.2}_{-0.4}$	2.2 ± 0.2
0.89	0.73	$2.5^{+1.4}_{-0.6}$	2.3 ± 0.2
0.89	0.75	$3.1^{+1.1}_{-0.4}$	2.6 ± 0.2
0.89	0.77	$3.2^{+1.3}_{-0.4}$	2.9 ± 0.2
0.89	0.79	$3.2^{+1.2}_{-0.4}$	3.0 ± 0.2
0.89	0.81	$3.0^{+1.2}_{-0.4}$	3.3 ± 0.2
0.89	0.83	$3.3^{+1.6}_{-0.6}$	3.6 ± 0.2
0.89	0.85	$3.6^{+1.2}_{-0.5}$	3.8 ± 0.2

TABLE VIII. The measured and predicted three-jet production cross section in every kinematically allowed bin in the Dalitz plane as a function of X_3 and X_4.

X_3	X_4	Measured Cross Section (pb)	NLO Cross Section CTEQ4M (pb)
0.89	0.87	$3.4^{+1.6}_{-0.5}$	4.7 ± 0.2
0.89	0.89	$1.9^{+0.8}_{-0.3}$	2.5 ± 0.2
0.91	0.55	$1.6^{+0.9}_{-0.4}$	1.4 ± 0.1
0.91	0.57	$2.0^{+1.2}_{-0.5}$	2.0 ± 0.2
0.91	0.59	$2.4^{+1.1}_{-0.3}$	2.3 ± 0.2
0.91	0.61	$2.6^{+1.4}_{-0.5}$	2.2 ± 0.2
0.91	0.63	$2.4^{+1.7}_{-0.8}$	2.1 ± 0.2
0.91	0.65	$2.4^{+1.5}_{-0.7}$	2.2 ± 0.2
0.91	0.67	$2.6^{+1.5}_{-0.4}$	2.5 ± 0.2
0.91	0.69	$2.5^{+1.3}_{-0.5}$	2.7 ± 0.2
0.91	0.71	$2.7^{+1.3}_{-0.6}$	2.3 ± 0.2
0.91	0.73	$3.1^{+1.4}_{-0.4}$	3.0 ± 0.2
0.91	0.75	$3.0^{+1.3}_{-0.5}$	3.3 ± 0.2
0.91	0.77	$3.5^{+1.8}_{-0.5}$	3.2 ± 0.2
0.91	0.79	$3.6^{+1.9}_{-0.6}$	3.6 ± 0.2
0.91	0.81	$3.3^{+1.6}_{-0.4}$	3.3 ± 0.2

TABLE IX. The measured and predicted three-jet production cross section in every kinematically allowed bin in the Dalitz plane as a function of X_3 and X_4. The prediction for the $X_3 = 0.93, X_4 = 0.53$ bin, for which the theoretical statistical uncertainty exceeds 20%, is not included.

X_3	X_4	Measured Cross Section (pb)	NLO Cross Section CTEQ4M (pb)
0.91	0.83	$3.3^{+1.2}_{-0.5}$	3.9 ± 0.2
0.91	0.85	$3.8^{+1.5}_{-0.5}$	5.0 ± 0.3
0.91	0.87	$4.6^{+1.4}_{-0.5}$	5.0 ± 0.3
0.91	0.89	$4.7^{+1.4}_{-0.5}$	5.4 ± 0.3
0.91	0.91	$2.2^{+0.7}_{-0.3}$	2.8 ± 0.2
0.93	0.53	$0.6^{+0.4}_{-0.2}$	$\cdots$
0.93	0.55	$2.7^{+1.4}_{-0.5}$	2.7 ± 0.2
0.93	0.57	$2.6^{+1.3}_{-0.4}$	2.2 ± 0.2
0.93	0.59	$2.8^{+1.3}_{-0.5}$	2.2 ± 0.2
0.93	0.61	$2.7^{+1.8}_{-0.7}$	2.3 ± 0.2
0.93	0.63	$2.6^{+1.3}_{-0.5}$	2.4 ± 0.2
0.93	0.65	$2.6^{+1.3}_{-0.4}$	2.3 ± 0.2
0.93	0.67	$3.0^{+1.4}_{-0.4}$	2.8 ± 0.2
0.93	0.69	$3.0^{+1.6}_{-0.5}$	3.0 ± 0.2
0.93	0.71	$3.4^{+1.7}_{-0.5}$	3.2 ± 0.2
0.93	0.73	$3.4^{+1.1}_{-0.3}$	3.5 ± 0.2

TABLE X. The measured and predicted three-jet production cross section in every kinematically allowed bin in the Dalitz plane as a function of X_3 and X_4. The prediction for the $X_3 = 0.95, X_4 = 0.53$ bin, for which the theoretical statistical uncertainty exceeds 20%, is not included.

X_3	X_4	Measured Cross Section (pb)	NLO Cross Section CTEQ4M (pb)
0.93	0.75	$3.3^{+1.6}_{-0.6}$	3.3 ± 0.2
0.93	0.77	$3.8^{+1.8}_{-0.4}$	3.7 ± 0.2
0.93	0.79	$4.1^{+1.7}_{-0.5}$	3.6 ± 0.2
0.93	0.81	$3.4^{+1.4}_{-0.5}$	4.2 ± 0.2
0.93	0.83	$3.9^{+1.6}_{-0.6}$	5.1 ± 0.3
0.93	0.85	$4.4^{+1.5}_{-0.6}$	5.5 ± 0.3
0.93	0.87	$4.4^{+1.8}_{-0.5}$	5.6 ± 0.3
0.93	0.89	$5.0^{+1.5}_{-0.9}$	6.4 ± 0.3
0.93	0.91	$4.9^{+1.3}_{-0.7}$	7.7 ± 0.3
0.93	0.93	$2.8^{+0.9}_{-0.4}$	3.2 ± 0.2
0.95	0.53	$1.2^{+0.6}_{-0.3}$	$\cdots$
0.95	0.55	$1.9^{+0.9}_{-0.3}$	1.5 ± 0.1
0.95	0.57	$2.1^{+1.1}_{-0.4}$	1.5 ± 0.1
0.95	0.59	$2.0^{+1.3}_{-0.6}$	1.4 ± 0.1
0.95	0.61	$1.9^{+1.1}_{-0.3}$	1.7 ± 0.1
0.95	0.63	$1.9^{+1.1}_{-0.5}$	1.9 ± 0.2

TABLE XI. The measured and predicted three-jet production cross section in every kinematically allowed bin in the Dalitz plane as a function of X_3 and X_4.

X_3	X_4	Measured Cross Section (pb)	NLO Cross Section CTEQ4M (pb)
0.95	0.65	$2.3^{+1.3}_{-0.3}$	1.8 ± 0.2
0.95	0.67	$2.2^{+1.2}_{-0.5}$	2.3 ± 0.2
0.95	0.69	$2.5^{+1.0}_{-0.3}$	2.6 ± 0.2
0.95	0.71	$3.1^{+1.6}_{-0.4}$	2.5 ± 0.2
0.95	0.73	$3.3^{+1.4}_{-0.5}$	3.2 ± 0.2
0.95	0.75	$3.7^{+1.9}_{-0.5}$	3.9 ± 0.2
0.95	0.77	$3.8^{+1.8}_{-0.6}$	3.8 ± 0.2
0.95	0.79	$4.0^{+1.5}_{-0.5}$	5.2 ± 0.3
0.95	0.81	$4.9^{+1.7}_{-0.7}$	5.4 ± 0.3
0.95	0.83	$5.4^{+2.0}_{-0.8}$	5.9 ± 0.3
0.95	0.85	$5.0^{+1.6}_{-0.6}$	6.2 ± 0.3
0.95	0.87	$5.7^{+1.6}_{-0.8}$	7.5 ± 0.3
0.95	0.89	$5.5^{+1.8}_{-0.9}$	7.9 ± 0.3
0.95	0.91	$5.4^{+1.4}_{-0.9}$	8.2 ± 0.3
0.95	0.93	$5.1^{+1.6}_{-0.8}$	7.1 ± 0.3
0.95	0.95	$1.9^{+0.8}_{-0.4}$	2.0 ± 0.2

TABLE XII. The measured and predicted three-jet production cross section in every kinematically allowed bin in the Dalitz plane as a function of X_3 and X_4. The prediction for the $X_3 = 0.97, X_4 = 0.53$ bin, for which the theoretical statistical uncertainty exceeds 20%, is not included.

X_3	X_4	Measured Cross Section (pb)	NLO Cross Section CTEQ4M (pb)
0.97	0.51	$0.2^{+0.1}_{-0.1}$	0.4 ± 0.1
0.97	0.53	$0.7^{+0.5}_{-0.2}$	...
0.97	0.55	$0.9^{+0.6}_{-0.2}$	0.3 ± 0.1
0.97	0.57	$0.8^{+0.5}_{-0.3}$	0.4 ± 0.1
0.97	0.59	$1.1^{+0.7}_{-0.2}$	0.3 ± 0.1
0.97	0.61	$0.9^{+0.7}_{-0.2}$	0.3 ± 0.1
0.97	0.63	$1.0^{+0.6}_{-0.2}$	0.9 ± 0.1
0.97	0.65	$1.1^{+0.8}_{-0.3}$	0.6 ± 0.1
0.97	0.67	$1.0^{+0.5}_{-0.2}$	0.8 ± 0.1
0.97	0.69	$1.4^{+0.7}_{-0.2}$	0.7 ± 0.1
0.97	0.71	$1.5^{+0.9}_{-0.4}$	0.8 ± 0.1
0.97	0.73	$1.5^{+0.8}_{-0.4}$	0.9 ± 0.1
0.97	0.75	$1.9^{+1.0}_{-0.4}$	1.5 ± 0.1
0.97	0.77	$1.9^{+1.0}_{-0.3}$	1.4 ± 0.1
0.97	0.79	$2.3^{+1.0}_{-0.3}$	2.2 ± 0.2
0.97	0.81	$2.8^{+1.2}_{-0.3}$	3.4 ± 0.2

TABLE XIII. The measured and predicted three-jet production cross section in every kinematically allowed bin in the Dalitz plane as a function of X_3 and X_4. Predictions for bins with $X_3 > 0.98$ are not included. The prediction for the $X_3 = 0.97, X_4 = 0.97$ bin, for which the theoretical statistical uncertainty exceeds 20%, is not included.

X_3	X_4	Measured Cross Section (pb)	NLO Cross Section CTEQ4M (pb)
0.97	0.83	$3.2^{+1.0}_{-0.4}$	4.0 ± 0.2
0.97	0.85	$3.9^{+1.3}_{-0.5}$	4.6 ± 0.2
0.97	0.87	$4.3^{+1.3}_{-0.6}$	6.5 ± 0.3
0.97	0.89	$5.4^{+1.2}_{-0.7}$	7.4 ± 0.3
0.97	0.91	$4.9^{+1.5}_{-0.9}$	7.7 ± 0.3
0.97	0.93	$3.8^{+1.2}_{-0.9}$	5.7 ± 0.3
0.97	0.95	$2.1^{+1.1}_{-0.7}$	3.0 ± 0.2
0.97	0.97	$0.3^{+0.2}_{-0.1}$	...
0.99	0.51	$0.0^{+0.1}_{-0.0}$	...
0.99	0.53	$0.0^{+0.1}_{-0.0}$	...
0.99	0.55	$0.1^{+0.1}_{-0.1}$	...
0.99	0.57	$0.1^{+0.0}_{-0.0}$	...
0.99	0.59	$0.1^{+0.1}_{-0.0}$	...
0.99	0.61	$0.1^{+0.1}_{-0.0}$	...
0.99	0.63	$0.1^{+0.1}_{-0.1}$	...
0.99	0.65	$0.1^{+0.1}_{-0.1}$	...

The theoretical prediction for the cross section, using CTEQ4M and all bins in the Dalitz plane but those with $X_3 > 0.98$, is $473 \pm 2(\text{stat.})^{+38}_{-66}(\text{scale})^{+21}_{-28}(\text{PDF})$ pb. The theoretical uncertainty associated with choice of renormalization and factorization scales, μ_R and μ_F respectively, is estimated by varying the scales, whose default value is E_T, to values of $E_T/2$ and $2E_T$ while keeping $\mu_R = \mu_F$. The theoretical uncertainty associated with choice of PDF is estimated from the spread in the predictions generated with other members of the CTEQ4 family. The measurement turned out not to be sensitive to the value of α_s as is also shown in [21]. The measured cross section, using all bins in the Dalitz plane but those with $X_3 > 0.98$, is $458 \pm 3(\text{stat.})^{+203}_{-68}(\text{syst.})$ pb. This is consistent with the theoretical prediction and with a previous CDF measurement [16] after corrections are made for the efficiencies of additional cuts introduced in this analysis. The measured cross section, using all bins in the Dalitz plane, is $466 \pm 3(\text{stat.})^{+207}_{-70}(\text{syst.})$ pb.

Tables I, II, III, IV, V, VI, VII, VIII, IX, X, XI, XII, XIII, and XIV summarize the measured cross section for every kinematically allowed bin in the Dalitz plane, including those for $X_3 > 0.98$. The measurements at high X_3 may provide useful constraints on future theoretical models in that region. The absolute predicted cross sections, using

TABLE XIV. The measured three-jet production cross section in every kinematically allowed bin in the Dalitz plane as a function of X_3 and X_4.

X_3	X_4	Measured Cross Section (pb)
0.99	0.67	$0.1^{+0.2}_{-0.1}$
0.99	0.69	$0.1^{+0.1}_{-0.1}$
0.99	0.71	$0.3^{+0.2}_{-0.1}$
0.99	0.73	$0.2^{+0.2}_{-0.1}$
0.99	0.75	$0.3^{+0.1}_{-0.1}$
0.99	0.77	$0.3^{+0.2}_{-0.1}$
0.99	0.79	$0.2^{+0.2}_{-0.1}$
0.99	0.81	$0.6^{+0.3}_{-0.2}$
0.99	0.83	$0.5^{+0.2}_{-0.1}$
0.99	0.85	$0.5^{+0.2}_{-0.2}$
0.99	0.87	$0.6^{+0.4}_{-0.1}$
0.99	0.89	$0.9^{+0.3}_{-0.1}$
0.99	0.91	$1.1^{+0.3}_{-0.3}$
0.99	0.93	$1.1^{+0.4}_{-0.3}$
0.99	0.95	$0.5^{+0.3}_{-0.2}$
0.99	0.97	$0.1^{+0.1}_{-0.1}$

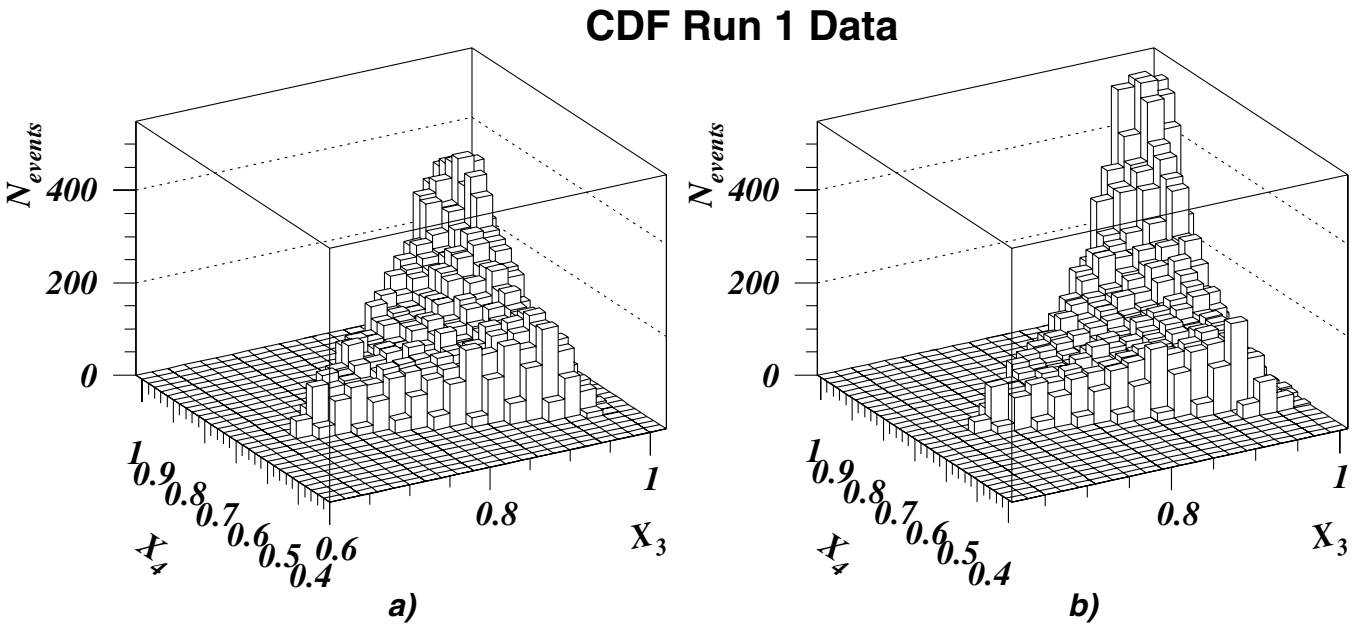

FIG. 2. The event density in the Dalitz plane for (a) the data and for (b) the prediction by the NLO Monte Carlo calculation with CTEQ4M, normalized to luminosity.

CTEQ4M and renormalization and factorization scales $\mu = E_T$, are also provided for bins with $X_3 \leq 0.98$. In a few bins, the predicted value is extremely small and dominated by theoretical uncertainties; for these bins no predicted value is quoted. The uncertainties on the measured values are the quadrature sum of statistical and systematic uncertainties; the uncertainties on the prediction reflect the statistics of the Monte Carlo sample.

In conclusion, we have presented the first comparison of three-jet event cross section variation across the Dalitz plane with predictions from a complete NLO QCD calculation. The total cross section is found to be $466 \pm 3(\text{stat.})^{+207}_{-70}(\text{syst.})$ pb. The data agree in absolute magnitude with theory and with our previous measurements. The shape of the theoretical and experimental distributions in the Dalitz plane differ somewhat; the difference may give an indication of the size of higher order corrections. It appears, for example, that up to NLO the theory predicts more soft radiation than the data have in the region where the primary partons are approximately back-to-back. The data, especially in the region above $X_3 = 0.98$ where a perturbative expansion is not reliable, may be useful input to theoretical models of gluon-emission processes.

We thank William Kilgore and Walter Giele for providing us with the code that computes the next-to-leading order calculation, and for their guidance concerning its use. We acknowledge the Center for High Performance Computing at the University of New Mexico and the University of Wisconsin Condor Project for providing a combined 26 000 CPU-hours for the Trirad NLO computations. We thank the Fermilab staff and the technical staffs of the participating institutions for their vital contributions. This work was supported by the U. S. Department of Energy and National Science Foundation; the Italian

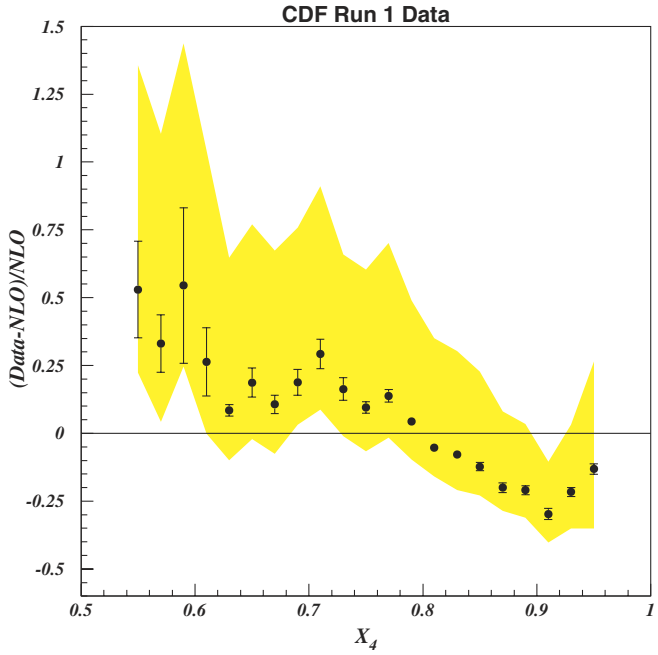

FIG. 3 (color online). The fractional difference between the data and the theoretical prediction, using CTEQ4M, as a function of X_4, averaged over X_3. The vertical bands show the systematic uncertainties. The error bars show the statistical uncertainties in cases where those are larger than the size of the symbol used. The prediction is normalized to the data to facilitate a comparison of the shapes of the distributions.

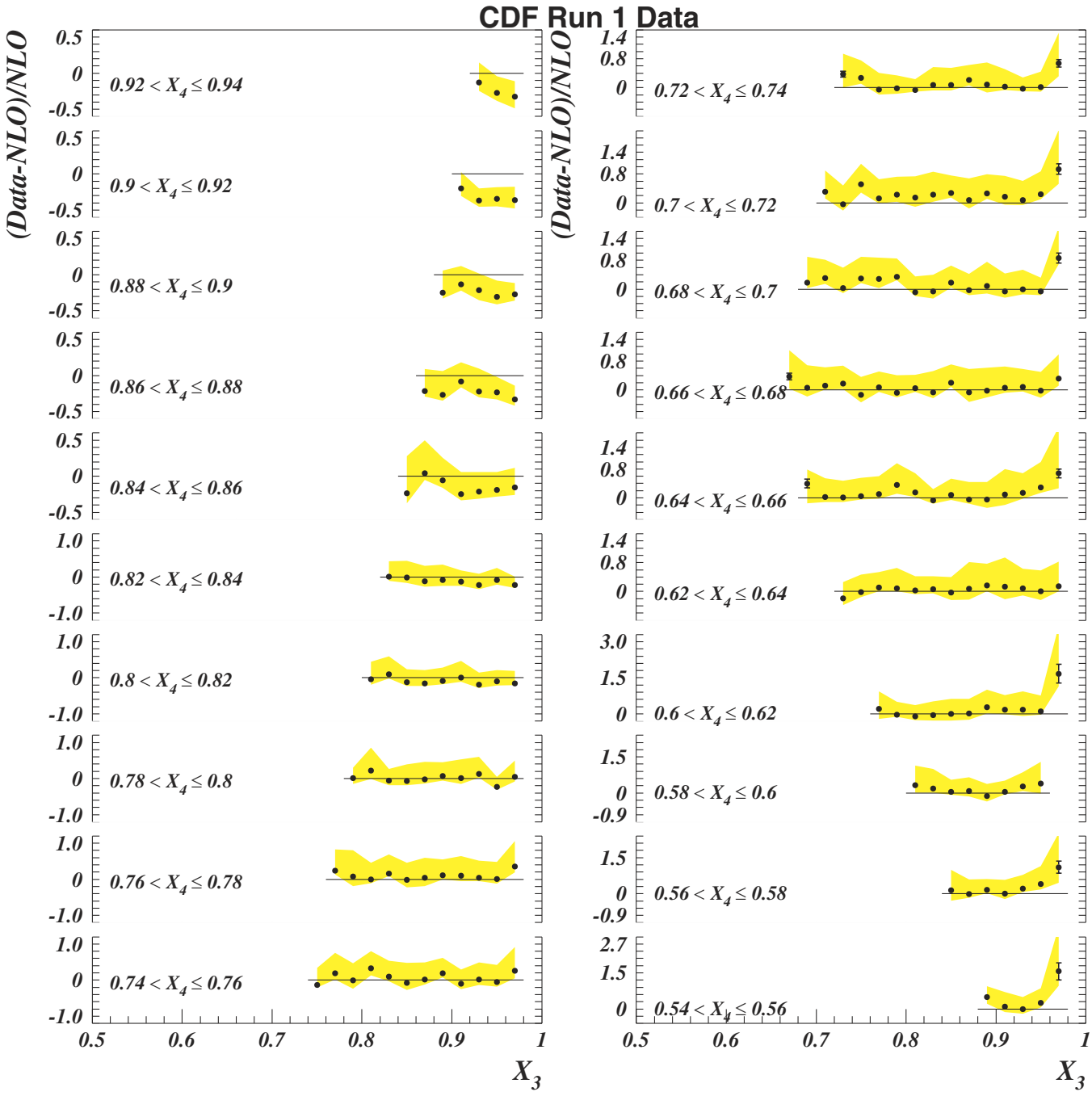

FIG. 4 (color online). The fractional difference between corrected data and the NLO prediction, using the CTEQ4M parton distribution function, as a function of X_3 for various X_4 bins. Error bars reflect statistical uncertainty for cases in which it is larger than the size of the symbol used. Shaded bands indicate systematic uncertainty. The prediction is normalized to the luminosity of the data.

Istituto Nazionale di Fisica Nucleare; the Ministry of Education, Science, Sports and Culture of Japan; the Natural Sciences and Engineering Research Council of Canada; the National Science Council of the Republic of China; the Swiss National Science Foundation; the A. P. Sloan Foundation; the Bundesministerium fuer Bildung und Forschung, Germany; and the Korea Science and Engineering Foundation.

[1] CDF Collaboration, F. Abe *et al.*, Nucl. Instrum. Methods Phys. Res., Sect. A **271**, 387 (1988).
[2] W. Kilgore and W. Giele, Report No. LANL-HEP-PH/ 9903361 (1999).
[3] C. Anastasiou *et al.*, Nucl. Phys. B **601**, 341 (2001); C. Anastasiou *et al.*, Nucl. Phys. B **605**, 486 (2001); E. W. N. Glover and M. E. Tejeda-Yeomans, J. High Energy Phys. 05 (2001) 010.
[4] CDF Collaboration, F. Abe *et al.*, Phys. Rev. D **45**, 1448 (1992).
[5] Z. Kunszt and E. Pietarinen, Nucl. Phys. B **164**, 45 (1980); T. Gottschalk and D. Sivers, Phys. Rev. D **21**, 102 (1980); F. Berends *et al.*, Phys. Lett. B **118**, 124 (1981).
[6] CDF Collaboration, F. Abe *et al.*, Phys. Rev. D **54**, 4221 (1996).
[7] G. Marchesini and B. Webber, Nucl. Phys. B **310**, 481 (1988).
[8] F. A. Berends *et al.*, Nucl. Phys. B **333**, 120 (1990); F. A. Berends *et al.*, Phys. Lett. B **232**, 266 (1990); F. A. Berends and H. Kuijf, Nucl. Phys. B **353**, 59 (1991).
[9] L. Balka *et al.*, Nucl. Instrum. Methods Phys. Res., Sect. A **267**, 272 (1988); S. Bertolucci *et al.*, Nucl. Instrum. Methods Phys. Res., Sect. A **267**, 301 (1988).
[10] UA1 Collaboration, G. Arnison *et al.*, Phys. Lett. B **158**, 494 (1985).
[11] S. Geer and T. Asakawa, Phys. Rev. D **53**, 4793 (1996).
[12] CDF Collaboration, F. Abe *et al.*, Phys. Rev. Lett. **62**, 1825 (1989).
[13] J. Huth *et al.*, in *Proc. 1990 Summer Study on High Energy Physics*, edited by E. Berger (World Scientific, Singapore, 1992), p. 134.
[14] CDF Collaboration, T. Affolder *et al.*, Phys. Rev. D **64**, 032001 (2001).
[15] W. B. Kilgore and W. T. Giele, Phys. Rev. D **55**, 7183 (1997).
[16] CDF Collaboration, F. Abe *et al.*, Phys. Rev. Lett. **80**, 3461 (1998).
[17] CDF Collaboration, F. Abe *et al.*, Phys. Rev. Lett. **77**, 438 (1996); CDF Collaboration, F. Abe *et al.*, Phys. Rev. Lett. **70**, 1376 (1993); CDF Collaboration, F. Abe *et al.*, Phys. Rev. Lett. **77**, 5336 (1996); CDF Collaboration, D. Cronin-Hennessy *et al.*, Nucl. Instrum. Methods Phys. Res., Sect. A **443**, 37 (2000).
[18] F. E. Paige and S. D. Protopopescu, BNL Report 29777, 1 (1981).
[19] T. Sjöstrand, Comput. Phys. Commun. **82**, 74 (1994).
[20] CTEQ Collaboration, H. L. Lai *et al.*, Phys. Rev. D **55**, 1280 (1997).
[21] See also J. Pumplin *et al.*, J. High Energy Phys. 07 (2002) 012.